Equation of state and jamming density for equivalent bi- and polydisperse, smooth, hard sphere systems

V. Ogarko[1, a)] and S. Luding[1, b)]
Multi Scale Mechanics (MSM), TS, CTW, University of Twente, PO Box 217, 7500 AE Enschede, The Netherlands.

(Received 24 October 2011; Accepted 25 February 2012)

We study bi- and polydisperse mixtures of hard sphere fluids with extreme size ratios up to 100. Simulation results are compared with previously found analytical equations of state by looking at the compressibility factor, Z, and agreement is found with much better than 1% deviation in the fluid regime. A slightly improved empirical correction to Z is proposed.

When the density is further increased, excluded volume becomes important, but there is still a close relationship between many-component mixtures and their binary, two-component equivalents (which are defined on basis of the first three moments of the size-distribution). Furthermore, we determine the size ratios for which the liquid-solid transition exhibits crystalline, amorphous or mixed system structure.

Near the jamming density, Z is independent of the size distribution and follows a -1 power law as function of the difference from the jamming density ($Z \to \infty$). In this limit, Z depends only on one free parameter, the jamming density itself, as reported for several different size distributions with a wide range of widths.
http://dx.doi.org/10.1063/1.3694030

PACS numbers: 64.30.-t, 81.40.Lm, 62.10.+s, 64.70.D-, 61.66.-f, 61.43.-j
Keywords: compressibility; crystal structure; density; equations of state; noncrystalline structure; solid-liquid transformations

I. INTRODUCTION

The hard-sphere model can be applied with some success for various physical phenomena and systems, like e.g., disorder-order transitions, the glass transition, dense granular flows and simple gases and liquids[1–7]. Kinetic theory describes the behavior of such particle systems, assuming that the particles are infinitely rigid and collisions are instantaneous[1,8], like in the hard-sphere model. In this paper we study the high density limit, where the caging-effect, that is, particles captured by their neighbors, becomes important in the dynamics of the global system and thus a free-volume theory needs to be formulated[9–15]. There exists no unique equation of state, valid for the intermediate densities, where the system changes from the disordered to the ordered state, since the system displays hysteresis and rate-dependence; for various theoretical approaches see Refs. 6, 16–25 and references therein.

In this study systems of particles of many different sizes are investigated in the high-density limit using theory and simulations. Fluid and jammed configurations of hard sphere mixtures are examined for various size distributions at slow compression rates[26–29]. Several authors proposed theories to compute the amorphus jamming density of binary and polydisperse hard sphere mixtures, see Refs. 30–34 and references therein. We construct a simple but physically reasonable model that relates the behavior of different hard sphere mixtures, even for metastable states. Additionally, we give accurate data for the jamming density as a function of size polydispersity, which is important for e.g. experiments on nonmonosized colloidal or granular systems.

In Sec. II, the theoretical ideas are introduced, which are needed to analyze the numerical results presented in Sec. III, before the results are summarized in Sec. IV.

II. THEORY

We consider a s-component thermalized mixture of N elastic smooth spheres, homogeneously placed in three-dimensional (3D) systems of volume V. Spheres are located at positions $\mathbf{r}_i$ with velocities $\mathbf{v}_i$, radii a_i and masses m_i. The kinetic energy $E_k = (1/2)\sum_{i=1}^{N} m_i \mathbf{v}_i^2$ is dependent on time via the particle velocities $\mathbf{v}_i$. For rigid spheres that do not interact except via an infinite repulsion on contact, i.e., with zero interaction / contact duration, the total energy is given by $E = E_k$, whereas for soft spheres the potential energy also has to be considered. The temperature in equilibrium hard-sphere systems is not a relevant parameter, since it does not affect the equilibrium configuration[28], it only scales time (or the free energy[35]). As a consequence, there is only one independent thermodynamic state variable, which can be either the reduced (dimensionless) pressure (so-called compressibility factor) $Z = PV/Nk_BT$ or the density (volume fraction) $\nu = 4\pi\sum a_i^3/(3V)$, related through the equation of state (EOS), where $k_BT = 2E/(3N)$ with the Boltzmann constant k_B.

a) Electronic mail: v.ogarko@utwente.nl
b) Electronic mail: s.luding@utwente.nl

A. Bidisperse systems

Let us consider a binary ($s = 2$) mixture of spheres with radii a_1 and a_2, with N_1 and N_2 the number of particles of each kind, and $N = N_1 + N_2$. Thus the mixture can be classified by only two parameters, the composition $n_1 = N_1/N$ and the size ratio $R = a_1/a_2$. The total volume fraction $\nu = \nu_1 + \nu_2$ is the last relevant system parameter, since the partial volume fractions $\nu_{1,2} = 4N_{1,2}\pi a_{1,2}^3/(3V)$ can be expressed[23] in terms of n_1 and R, using the dimensionless moments

$$A_k = n_1 + (1 - n_1)R^{-k} = \langle a^k \rangle / a_1^k, \tag{1}$$

where $\langle a^k \rangle = n_1 a_1^k + n_2 a_2^k$. With this, one has $\nu_1 = n_1\nu/A_3$ and $\nu_2 = (1 - n_1)\nu/(R^3 A_3)$.

A calculation in style of Jenkins and Mancini, see Refs. 36 and 37, leads to the partial translational pressures $p_i^t = 2n_i E/(3V)$ for species i and to the collisional pressures $p_{ij}^c = \pi N_1 N_2 g_{ij} a_{ij}(1 + r_{ij})T/(3V^2)$ with the particle correlation function g_{ij} evaluated at contact, and $a_{ij} = a_i + a_j$. In the following, for simplification the inter-species restitution coefficients r_{ij} are set to unity (elastic case), $r_{11} = r_{12} = r_{22} = 1$. The particle correlation functions g_{ij} from Ref. 37–40, are here expressed in terms of $A_{2,3}$, R and ν:

$$g_{11} = \frac{1}{1-\nu} + \frac{3\nu\frac{A_2}{A_3}}{2(1-\nu)^2} + \frac{(\nu\frac{A_2}{A_3})^2}{2(1-\nu)^3}, \tag{2}$$

$$g_{22} = \frac{1}{1-\nu} + \frac{3\nu\frac{A_2}{RA_3}}{2(1-\nu)^2} + \frac{(\nu\frac{A_2}{RA_3})^2}{2(1-\nu)^3}, \tag{3}$$

$$g_{12} = \frac{1}{1-\nu} + \frac{3\nu\frac{A_2}{(1+R)A_3}}{(1-\nu)^2} + \frac{2(\nu\frac{A_2}{(1+R)A_3})^2}{(1-\nu)^3}. \tag{4}$$

Thus, the global pressure in the mixture is:

$$\begin{aligned} p^m &= p_1^t + p_2^t + p_{11}^c + 2p_{12}^c + p_{22}^c \\ &= \frac{2E}{3V}\left[1 + \frac{\nu}{2\langle a^3\rangle}(g_{11}a_{11}^3 n_1^2 + 2g_{12}a_{12}^3 n_1 n_2 + g_{22}a_{22}^3 n_2^2)\right] \\ &= \frac{2E}{3V}\left[1 + 4\nu g_{\text{eff}}(\nu)\right]. \end{aligned} \tag{5}$$

Like done for 2D systems in Ref. 23, the effective correlation function $g_{\text{eff}}(\nu)$ can be expressed in term of the dimensionless moments:

$$O_1 = \frac{\langle a\rangle\langle a^2\rangle}{\langle a^3\rangle} \text{ and } O_2 = \frac{\langle a^2\rangle^3}{\langle a^3\rangle^2} \tag{6}$$

so that (see Appendix A)

$$g_{\text{eff}}(\nu) = \frac{(1-\nu)^2 + 3O_1(1-\nu) + O_2(3-\nu)\nu}{4(1-\nu)^3}. \tag{7}$$

Then the equation of state for mono- and bidisperse systems reads:

$$Z = 1 + 4\nu g_{\text{eff}}(\nu). \tag{8}$$

Note that in the monodisperse case all g_{ij} and $g_{\text{eff}}(\nu)$ are identical to the pair distribution function at contact $g_{\text{CS}}(\nu) = (1 - \nu/2)/(1 - \nu)^3$, proposed by Carnahan and Starling (CS)[41], since $R = 1$, $A_k = O_{1,2} = 1$ (using the relation $Z_{\text{CS}} = 1 + 4\nu g_{\text{CS}}$ (Ref. 38)). The Carnahan-Starling pair distribution function is quite accurate at low and moderate volume fractions, but does not show the reported divergence due to excluded volume effects at the close packing volume fraction[42,43].

B. Polydisperse systems

In the case of a polydisperse mixture ($s = N \to \infty$) in which the sphere radius is distributed according to some probability density function $f(a)$, $\langle a^k \rangle \equiv \int a^k f(a) da$ is the k-th moment of the size distribution. By just using these moments, the function $g_{\text{eff}}(\nu)$ from Eq. (7) is well defined also for multi-component systems of spheres. It turns out that the equation of state (8) coincides with the well-known Boublík, Mansoori, Carnahan, Starling, and Leland (BMCSL) equation of state proposed for mixtures[38,44]:

$$Z_{\text{BMCSL}} = \frac{1}{1-\nu} + O_1\frac{3\nu}{(1-\nu)^2} + O_2\frac{\nu^2(3-\nu)}{(1-\nu)^3}. \tag{9}$$

There are several modified equations of state for multicomponent mixtures in the literature, which require the knowledge of the equation of state for a one-component system[20]. First, we consider Santos *et al.*'s equation of state, based on the Carnahan-Starling equation of state:

$$Z_{\text{SCS}} = Z_{\text{BMCSL}} + (O_1 - O_2)\frac{\nu^3}{(1-\nu)^3}. \tag{10}$$

Second, following Santos *et al.*'s procedure based on the Carnahan-Starling-Kolafa (CSK) equation of state, $Z_{\text{CSK}} = [1 + \nu + \nu^2 - 2\nu^3(1+\nu)/3]/(1-\nu)^3$[45], one gets

$$Z_{\text{SCSK}} = Z_{\text{SCS}} + (O_1 + O_2)\frac{\nu^3(1-2\nu)}{6(1-\nu)^3}. \tag{11}$$

Third, Boublík extended the CSK equation of state to mixtures[46], yielding:

$$Z_{\text{BCSK}} = Z_{\text{BMCSL}} + O_2\frac{\nu^3(1-2\nu)}{3(1-\nu)^3}. \tag{12}$$

Although we could consider the extensions of other equations of state[47], for the sake of simplicity we will restrict our analysis to the above mentioned equations of state.

C. Discussion

It is interesting to observe that all the equations of state considered in Sec. II B are functionals of the particle size distribution (PSD) only through its dimensionless moments O_1 and O_2. Therefore, we study and discuss the properties of O_1 and O_2. It can be shown that $0 < O_1 \leq 1$ and $O_1^2 \leq O_2 \leq O_1$ for any size distribution function (see Appendix B). This property makes it convenient to characterize a size distribution by a point on the O_1O_2 plane.

We can see that O_1 is the ratio of the arithmetic mean diameter to the Sauter mean diameter, and it is a measure of the *broadness* of the PSD[48], i.e., $O_1 = D_{10}/D_{32}$, with $D_{pq} = 2(\int a^p f(a)da / \int a^q f(a)da)^{1/(p-q)}$. Correspondingly, $O_2 = (D_{20}/D_{32})^2$ is another measure for shape and width of the PSD. Those combined size-descriptors were already used as early as 1979 to model systems like polydisperse sprays[49].

In the bidisperse case the system of equations (6) can be solved analytically in terms of the variables n_1 and R, yielding a unique solution: $n_1^{\text{bi}}(O_1, O_2)$ and $R^{\text{bi}}(O_1, O_2)$ (see Appendix C). This means that for any given polydisperse system we can construct an *"equivalent"* bidisperse system, which has the same equation of state in the fluid regime. We use this in Sec. III to check how the compressibility factor and the jamming density of polydisperse systems are related to those of their bidisperse equivalents. Earlier, equivalent binary mixtures were used to investigate a slightly polydisperse hard sphere crystal in Ref. 50, while here we will show that they can be used to model widely polydisperse fluids and glasses at all densities, which is in the spirit of what Santos *et al.* call the "universality" ansatz, see Refs. 51–53 and references therein.

III. COMPARISON WITH SIMULATIONS

Since we are interested in the behavior of rigid particles, we perform event-driven molecular dynamics simulations using the modification of the Lubachevsky-Stillinger algorithm[54] as the primary tool for our investigations[28,55,56]. The system consists of a cubic cell, with periodic boundary conditions, which are imposed to simulate an infinite system, i.e., a statistically homogeneous medium. The compressibility factor is calculated from the total exchanged momentum in all interparticle collisions during a certain short time period Δt, given by 400 events per particle. By growing the size of the particles linearly in time with a growing rate Γ one can change the volume fraction (for details see Appendix D). Over time the additional energy created during collisions would accelerate the particles, but this is avoided by periodic rescaling of the average particle velocity to hold the mean temperature constant[55], such that the total change in kinetic energy of the system is kept small (below 1%). If the growing is sufficiently slow, the system will be in approximate equilibrium during the densification and one can rather efficiently gather quasi-equilibrium data as a function of density[6,57]. The number of particles N used in most simulations is $16^3 = 4096$, if not explicitly stated otherwise. In order to improve the performance of neighborhood search the ideas of a multilevel contact detection algorithm[58] can be used, but were not implemented here.

A. Particle size distributions

The following types of particle size distributions are used: (i) uniform size distribution; (ii) uniform volume distribution, i.e., the probability distribution of the volume of the particles is constant; (iii) systems constructed by mapping the aforementioned polydisperse systems to bidisperse ones (see Sec. II C for details).

For a given size distribution, we denote the ratio between the maximum and the minimum particle radius as ω. Therefore, $\omega = 1$ corresponds to the monodisperse case, i.e., all sizes are equal, and in our convention $\omega \geq 1$. Further in the paper when we use ω for bidisperse systems we mean the extreme size ratio of the equivalent polydisperse system, while for the true size ratio we use R^{bi}. Examples and analytical expressions for O_1 and O_2 as function of ω for the considered size distributions are shown in Appendix E.

The use of a single variable, i.e., the size ratio ω, excludes continuous distributions like log-normal, for which one has to use O_1 and O_2 for classification, see Appendix E. The size-distributions used here, due to their sharp edges with well defined ω, could be obtained by ideal sieving from wider, smooth continuously distributed realistic distributions.

The sizes of particles of polydisperse systems are drawn from the particle size distribution function using the systematic sampling approach[59,60]. It guarantees a more evenly spread sample, i.e., there will always be large particles, even if they are rare, like in the case of the uniform volume distribution.

B. Equation of state in the fluid regime

In Fig. 1 we show the compressibility factor Z from simulations scaled by the BMCSL, SCS, SCSK and BCSK equations of state for different densities and for different size distributions. Note, that in the monodisperse case ($O_1 = O_2 = 1$) $Z_{\text{CS}} = Z_{\text{BMCSL}} = Z_{\text{SCS}}$ and $Z_{\text{SCSK}} = Z_{\text{BCSK}}$.

We observe for monodisperse systems that the deviation of the compressibility factor from all considered theories is below 0.3% (a) in the volume fraction region of $0 < \nu < 0.54$. The deviation is well below 1% in the volume fraction region of $0 < \nu \leq 0.6$ for polydisperse systems: for uniform size, with $\omega = 5$ (b), uniform size, with $\omega = 100$ (c), and uniform volume, with $\omega = 4$ (d),

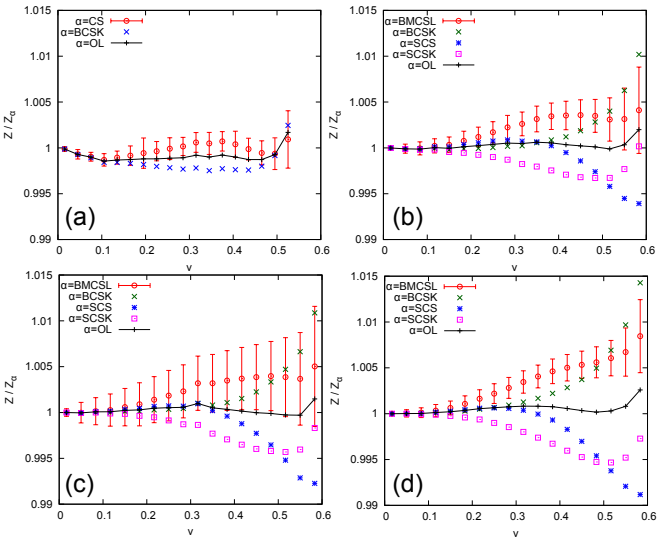

FIG. 1. (Color online) The quality factor, i.e., the numerical Z scaled by the theoretical predictions for different densities and for different size distributions (a) monodisperse, and polydisperse with (b) uniform size, $\omega = 5$, (c) uniform size, $\omega = 100$, and (d) uniform volume, $\omega = 4$. The growth rate for all data is $\Gamma = 16 \times 10^{-6}$. The error bars indicate the standard deviation of the quality factor within an averaging bin. The error bars are shown only for the BMCSL EOS since in the other cases they have the same trend and magnitude.

distributions, respectively. This indicates that the number of particles is large enough to realistically represent the respective size distributions to suppress possible effects of finiteness of the system. The uniform volume distribution does not allow to properly realize wider distributions, due to the small sample size, $N = 4096$.

Based on all these results, we propose a more accurate equation of state for the fluid regime, which is simply the arithmetic average of Santos *et al.*'s and Boublík's extensions:

$$Z_{\mathrm{OL}} = \frac{1}{2}(Z_{\mathrm{SCS}} + Z_{\mathrm{BCSK}}). \tag{13}$$

Equation (13) is more accurate at intermediate volume fractions $0.20 - 0.60$ and is almost identical to the other forms for lower volume fractions. For all systems, with $\nu \leq 0.60$, presented in Fig. 1, Z_{OL} performs better than 0.2% except for the monodisperse case data, for $\nu > 0.54$, due to crystallization.

Our simulations also confirm that for $\nu < 0.54$ the agreement in the compressibility factor between the considered polydisperse systems and their bidisperse equivalents (defined in Sec. II C) is of order of 0.1% for $\omega \leq 50$ (data not shown).

In the following we show what happens at higher volume fractions.

C. How much disorder is necessary to avoid order?

According to Alder *et al.*[28,61], monodisperse hard-sphere systems undergo a first-order fluid-solid phase transition, characterized by a *melting point*, i.e., the density at which the crystal thermodynamically begins to melt, and a *freezing point*, i.e., the density at which the fluid thermodynamically begins to freeze. In this subsection, we investigate how much polydispersity is needed to avoid partial crystallization, complementing an earlier study in 2D (Ref. 24) and 3D (Ref. 62) as also studied in experiments on colloids[63].

Since the compressibility factor increases very rapidly at densities higher than the freezing point, we plot the estimated jamming density $\phi_J = \nu/(1 - d/Z)$ instead of the compressibility factor, inspired by[28], as shown in Fig. 2, since $\phi_J(Z \to \infty) = \nu$. The estimated jamming density ϕ_J here is derived from the free-volume EOS for a d-dimensional system[12]:

$$Z_{\mathrm{fv}} = \frac{d}{1 - \nu/\phi_J}. \tag{14}$$

In Fig. 2, ϕ_J is plotted against ν for different systems with uniform size distribution. Data agree perfectly with the fluid theory before the particle system changes from the fluid state to the state of coexistence of fluid and solid, as indicated by a sharp increase (jump) above the fluid prediction, see Fig. 2(a). The jumps are due to partial crystallization observed for size ratios $1 \leq \omega \lesssim 1.2$ but not for larger ω. (It must be noted that for the system with $\omega = 1.2$, partial crystallization is observed not for every run, as shown in Fig. 2(a) for two runs with random initial velocities, i.e., from six runs we found that four systems exhibit partial crystallization, while two systems do not.) Near the critical size ratio, $\omega_c \approx 1.20 \pm 0.02$, where ordering effects disappear, also the history and fluctuations of the system play an important role.

For the critical polydispersity, a simple model which agrees with our findings was proposed[64], inspired by Lindemann's melting criterion: a crystal melts when the thermally-induced root-mean-square displacement of an atom or particle reaches a characteristic fraction of the typical interparticle spacing[3]. Our findings also agree with the criterion for stability of the polydisperse crystal based on free energy minimization[65].

It should be noted that it is possible to observe a polydisperse crystal also for large size ratios, if the particles are allowed to redistribute for very long time[35,66]. In this case, different annealed phase behavior is expected at high densities[65]. Self-diffusion can occur and spheres can crystallize into multiple crystal phases (domains) each containing spheres of a different size.

In the monodisperse case the *metastable freezing point*, i.e., the density of partial crystallization of the densified fluid, is very close to 0.54, which is in good agreement with data from Refs. 6, 28, and 68. This should not be confused with the freezing point, which implies the stable

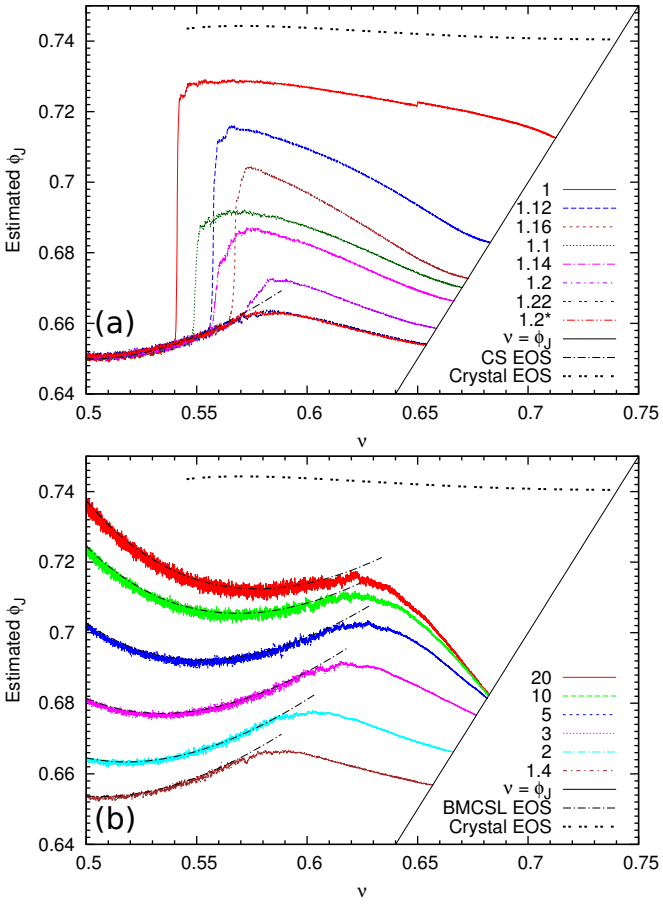

FIG. 2. (Color online) The estimated jamming density ϕ_J as a function of volume fraction ν for systems with uniform size distribution. Shown are systems of 4096 spheres with various size ratios ω. In (a) ω, given in the inset, corresponds to decreasing ϕ_J (top-to-bottom), and in (b) increasing ω corresponds to bottom-to-top. Also plotted are the fluid theory (BMCSL EOS) and the approximation for the crystal phase[67]. The used growth rate here is $\Gamma = 8 \times 10^{-6}$. For $\omega = 1.2$ data for two different runs are shown, marked with 1.2 and 1.2*.

thermodynamic point and occurs at about 0.49 as determined from a number of different simulations[69,70] and free energy calculations[71]. While a metastable freezing point depends on the compression rate, the freezing point does not. The location of the metastable freezing point, ν_f, is shifted to higher density with increasing polydispersity. Taken from a few representative simulations, values are $\nu_f = 0.540, 0.548, 0.556, 0.557, 0.565, 0.573$ for $\omega = 1, 1.1, 1.12, 1.14, 1.16, 1.2$, respectively, fluctuating with different runs (± 0.005). The latter trend reverses (decreasing ν_f) for another type of crystallization which we observe in the bidisperse systems with (relatively) large size ratios, see Fig. 3. This is discussed in more detail in Sections III D and III E. In contrast, there is no strong dependence of the (final) jamming density on ω for partially crystallized systems, since crystallization is a stochastic nucleation process, i.e., different runs of the same system with random initial particle velocities will lead to different jamming densities (data not shown). The trends in Fig. 2(b) show that the larger ω, the larger the density at which disordered systems (not crystallized) deviate from the fluid theory (the sharp increase of ϕ_J relative to the fluid theory turns to a smooth decrease). In addition, for such systems the jamming density is increasing with ω, which is discussed in more detail in Sec. III E. Finally, all curves end at the identity line $\phi_J = \nu$ at densities well below the perfect crystal EOS[67], for which $\phi_J = \nu \approx 0.74$ would be expected (for mono-disperse systems).

We checked (data not shown) that the jumps in ϕ_J vanish around $\omega \approx 1.2$ ($R^{\text{bi}} \approx 1.1$) also for other size distributions, which are defined in Sec. III A. We only remark that the bidisperse systems – equivalent to systems with uniform volume distribution – show some fine structure around the jumps, which we do not discuss here for the sake of brevity.

In Fig. 4, systems with uniform size distribution shown for different size ratios ω. It can be seen how the ordering disappears as the size ratio increases.

In Fig. 5 bidisperse systems corresponding to uniform size distributions are shown for different size ratios, i.e., with (relatively) small size ratios just below the crystallization ratio, Fig. 5(a), just above, Fig. 5(b), and with (relatively) large size ratios just below and above partial (single species) crystallization in Figs. 5(c) and 5(d), respectively. Note that changing of the polydispersity from 10% (a) to 11% (b) changes the physical state of the system a lot, so that we can see the difference even by the eye, which is quite remarkable. This is consistent with results from Ref. 72, where for a binary mixture with a size ratio 1.111 and $n_1 = 0.5$ crystallization was almost totally suppressed.

In Sec. III E we investigate the order-disorder transition for many different size distributions in more detail using another criterion to measure partial crystallization.

D. Bidisperse versus polydisperse

The aim of this subsection is to compare the equation of state of polydisperse systems and their bidisperse equivalents at volume fractions where fluid theory is not valid, i.e., in their "glassy" states or in coexistence of fluid and solid phases. Figure 6 shows ϕ_J as a function of volume fraction for a few systems with uniform size distribution and their bidisperse equivalents, 6(a), and for systems with uniform volume distribution and their bidisperse equivalents, 6(b).

While for small size ratios, $\omega \lesssim 1.2$, ordering / crystallization occurs, see Fig. 2(a), for moderate size ratios, $1.2 \lesssim \omega \lesssim 4$, the estimated jamming density of the considered polydisperse systems and their respective bidisperse equivalents are within 1%, where the bidisperse data are slightly below. Thus, one can reduce

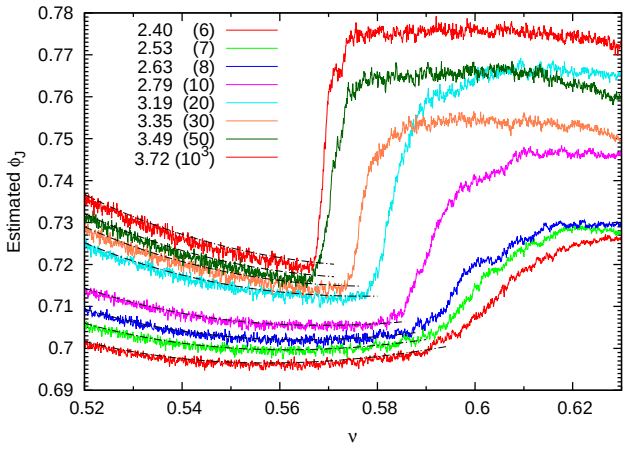

FIG. 3. (Color online) The estimated jamming density ϕ_J as a function of volume fraction ν for bidisperse systems corresponding to uniform size distribution. Increasing ω corresponds to bottom-to-top, with growth rate $\Gamma = 16 \times 10^{-6}$. The (metastable) freezing density is decreasing with increasing size ratio. The BMCSL EOS are shown by dash-dotted lines.

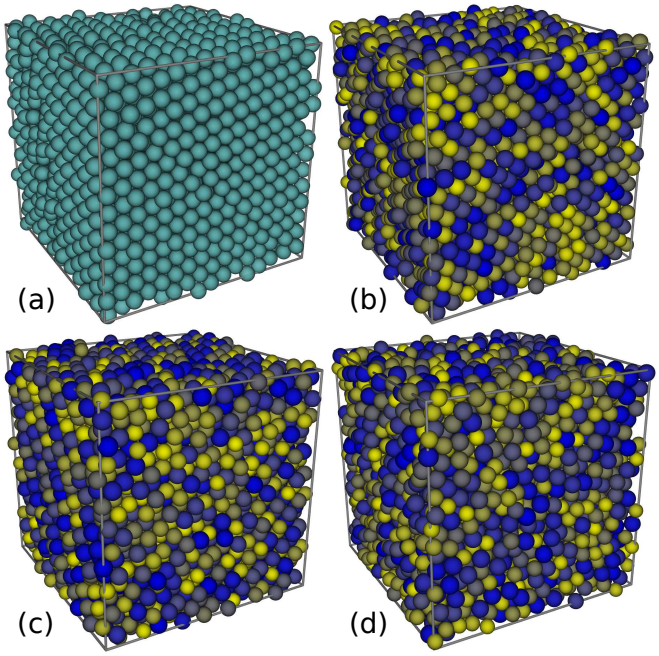

FIG. 4. (Color online) Particle systems with uniform size distribution with different size ratios at densities very close to jamming. Size ratios are $\omega = 1$ (a), $\omega = 1.12$ (b), $\omega = 1.18$ (c), and $\omega = 1.22$ (d). The order-disorder transition can be clearly seen as the size ratio increases. Color is by relative size, i.e., yellow (light) corresponds to small particles, and blue (dark) corresponds to big ones. The used growth rate to reach these configurations was $\Gamma = 8 \times 10^{-6}$.

mixtures to two-component (binary) systems, which have

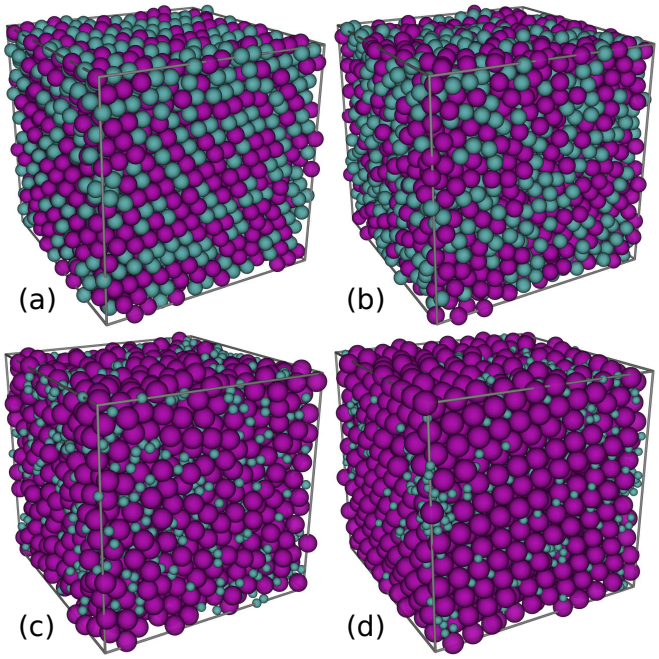

FIG. 5. (Color online) Particle systems with bidisperse size distribution corresponding to a uniform size distribution, i.e., $n_1 = 1/2$, with different size ratios at densities very close to jamming. Size ratios are $R^{\text{bi}} \approx 1.100$ ($\omega = 1.18$) (a), $R^{\text{bi}} \approx 1.111$ ($\omega = 1.2$) (b), $R^{\text{bi}} \approx 2.060$ ($\omega = 4$) (c), and $R^{\text{bi}} \approx 2.404$ ($\omega = 6$) (d). The order-disorder transition can be clearly seen. Note that in (d) also some signs of segregation / clusterization of small particles can be seen, though investigation of this is beyond the scope of this paper.

similar physics, even when the system densities are above the fluid-regime.

The equivalency of two- and many-component mixtures breaks down in the case of uniform size distribution as polydispersity (width) increases, e.g., for $\omega = 6$ ($R^{\text{bi}} \approx 2.4$, $n_1^{\text{bi}} = 1/2$), due to partial crystallization of the big particles in the bidisperse system, as it can also be seen in Fig. 5(d). This is consistent with results from Ref. 73, where the structure of binary hard sphere mixtures is studied in more detail. This kind of partial crystallization happens since the small particles fit into interstices of a crystal made of the large particles[64]. Such "colloidal alloy" structures have been observed both in naturally-occurring opals[74] and synthetic colloids[75,76].

In the case of bidisperse distributions corresponding to uniform volume distributions, we did not observe strong evidence of partial crystallization in the $1.18 \leq \omega \leq 10$ ($1.10 \lesssim R^{\text{bi}} \lesssim 3.89$) range, even though a bit of restructuring for $\omega \geq 5$, see Fig. 6(b), seems to happen.

In the inset of Fig. 6(b) the zoomed data for $\omega = 8$ are plotted, showing that the (final) jamming density can change (jump) also very close to the identity line $\phi_J = \nu$, indicating considerable re-structuring even very close to jamming.

In Subsection III E we determine more precisely the

range of size ratios for which systems show crystallization and/or partial single-species ordering.

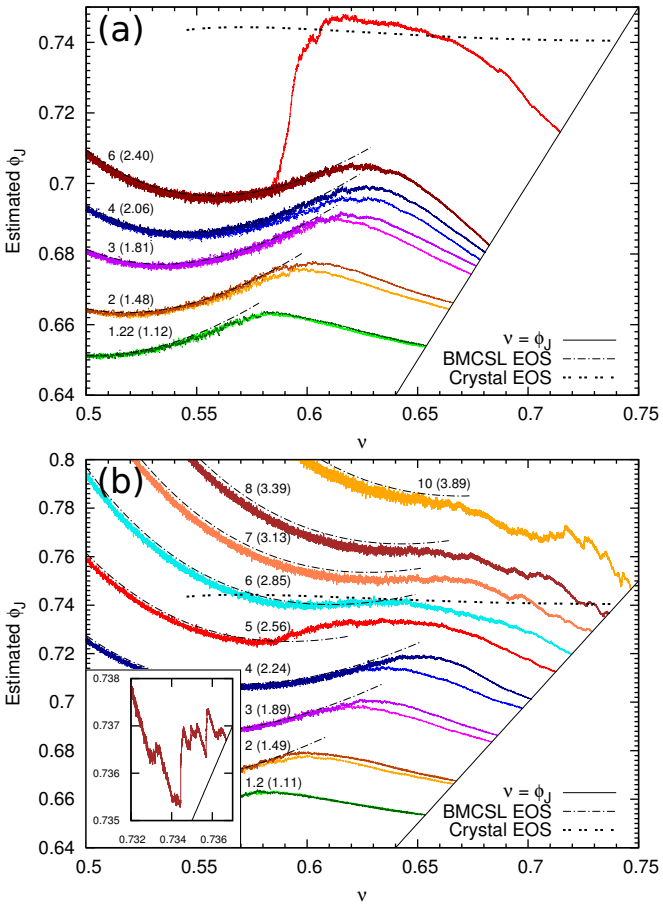

FIG. 6. (Color online) The estimated jamming density ϕ_J as a function of volume fraction ν for systems with (a) uniform size distribution and their bidisperse equivalents, using $\Gamma = 8\times10^{-6}$, and for systems with (b) uniform volume distribution and their bidisperse equivalents, using $\Gamma = 16 \times 10^{-6}$. Size ratios ω and R^{bi} are displayed in the inset, where the latter is given in brackets. Also plotted are the fluid theory (BMCSL EOS) and the approximation for the crystal phase[67]. Data for polydisperse systems in (b) are shown for $\omega \leq 4$. In the inset of (b) the zoomed data for $\omega = 8$ are shown.

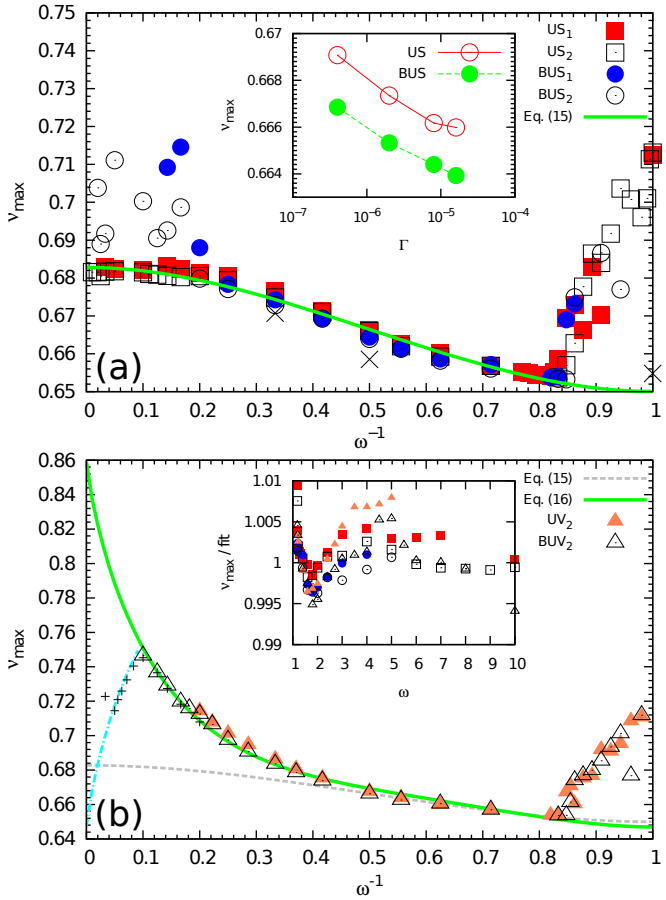

FIG. 7. (Color online) The maximum density $\nu_{\max}$ as a function of the inverse size ratio ω^{-1} for different size distributions and for different compression rates, in the inset subscript 1 corresponds to the reference growth rate $\Gamma = 8 \times 10^{-6}$, and subscript 2 corresponds to $\Gamma = 16 \times 10^{-6}$, i.e. two times faster. Size distributions are (a) uniform size distribution (US) and their bidisperse equivalents (BUS), or (b) uniform volume (UV) and their bidisperse equivalents (BUV). The size ratio ω corresponds to the polydisperse systems, while bidisperse ones are constructed using C. Results for BUV systems with $N = 8192$, using $\Gamma = 16 \times 10^{-5}$, are shown as pluses in (b), which are fitted for $\omega \geq 10$ by Eq. (16) with swapped values of ϕ_{RCP} and $\nu^{\infty}_{\max}$ (dash-dotted line). The left most point (+, $\omega = 30$) is higher than expected because of partial crystallization, setting in also here at very large ω. Results from Ref. 83 obtained by compression of soft frictionless particles with a uniform size distribution are shown as crosses in (a). In the inset of (a), $\nu_{\max}$ is plotted for different growth rates Γ for the uniform size distribution ($\omega = 2$) and their bidisperse equivalent ($R^{\text{bi}} \approx 1.48$). In the inset of (b), the deviation of data from the fits is shown with corresponding symbols.

E. Towards the jamming density

In this subsection, we investigate the maximum density $\nu_{\max}$ as a function of polydispersity. By maximum density we mean the density obtained after long-term (slow) compression, i.e., further compression for a time period about 4×10^5 events per particle does not increase the density, possibly due to numeric limits. The average compressibility factor of the final (jammed) systems is typically $Z \geq 10^{13}$. (In Subsection III G we will also verify that the (related) difference between obtained densities $\nu_{\max}$ and the *true jamming densities*, i.e., the densities where the compressibility factor becomes infinity, is at most 10^{-13}.)

In the amorphous regime ϕ_J decreases (Z increases) relative to the fluid prediction, due to excluded volume effects. In Figs. 2 and 6, ordering / crystallization was characterized by an increase of ϕ_J above the fluid pre-

diction (i.e. a decrease of Z below). Now, we also relate this to the change of behavior of $\nu_{\max}$, which is consistent with Ref. 29.

Figure 7 shows the maximum density $\nu_{\max}$ as a function of the inverse size ratio ω^{-1} for different size distributions and for different compression rates. The size ratio ω corresponds to polydisperse systems, while equivalent bidisperse ones are constructed using formulas (C1) and (C2). Firstly, we see that for small polydispersity $\omega^{-1} \gtrsim 0.85$, i.e., $\omega \leq 1.18$ ($R^{\text{bi}} \lesssim 1.100$), all the considered systems display (partial) crystallization or ordering effects, characterized by a jump (discontinuous increase) in $\nu_{\max}$ with ω^{-1}. Note that the bidisperse systems corresponding to uniform volume distributions do not crystallize for $\omega = 1.18$ (checked for three different runs), but for slightly smaller $\omega \leq 1.17$ ($R^{\text{bi}} \lesssim 1.095$). Partial crystallization of this type (small ω) can be seen by the eye in Fig. 5(a).

In the $1.22 \leq \omega \leq 4$ range there is no (partial) crystallization observed for any of the considered systems. Furthermore, the maximum density of polydisperse systems is just slightly larger (within 0.5%) than for their bidisperse equivalents, see the inset in Fig. 7(b). Note that in the case of uniform volume distributions, larger ω cannot be properly realized for too small $N = 4096$, so we do not show results for $\omega > 5$.

For larger ω, i.e., $\omega \geq 5$, bidisperse systems corresponding to uniform size distributions undergo partial crystallization of the large species ($R^{\text{bi}} \gtrsim 2.25$), which was discussed in the previous subsection.

As already evident in Fig. 6, the system with uniform volume distribution and their bidisperse equivalents pack "better" and reach much larger $\nu_{\max}$, see Fig. 7(b), when compared to 7(a), even without apparent partial (species) crystallization[77].

In contrast to their bidisperse counterparts, polydisperse systems with uniform size distribution do not show any signs of crystallization for $\omega \geq 1.22$, and the maximum density converges with increasing polydispersity to $\nu^{\infty}_{\max} \approx 0.6828 \pm 0.0004$, seemingly not changing much even for extremely wide distributions.

From our data, for uniform size distribution $\nu_{\max}$ can be fitted by a function of ω:

$$\nu_{\max}(\omega) = \nu^{\infty}_{\max} - (\nu^{\infty}_{\max} - \phi_{\text{RCP}})(3\omega^{-2} - 2\omega^{-3}), \quad (15)$$

where the random close packing density ϕ_{RCP} is taken to be 0.65, as also predicted by cell theory[78]. The deviation is within $\pm 0.5\%$ for all data $\omega \gtrsim 1.2$, see the inset in Fig. 7(b), and we enforced the derivative $\nu'_{\max} \equiv 0$ for $\omega^{-1} \to 1$.

The maximum density of systems with uniform volume distribution and their bidisperse equivalents can be fitted by a function of ω in the range $1.2 \leq \omega \leq 10$:

$$\nu_{\max}(\omega) = \nu^{\infty}_{\max} - (\nu^{\infty}_{\max} - \phi_{\text{RCP}})(\omega^{-1} - \omega^{-2} + \omega^{-3})(1 - \log \omega^{-2}), \quad (16)$$

where $\phi_{\text{RCP}} = 0.647$ and $\nu^{\infty}_{\max} = 0.859$, with deviation within $\pm 1\%$, see the inset in Fig. 7(b), and we enforced the derivative $\nu'_{\max} \equiv 0$ for $\omega^{-1} \to 1$. The bidisperse equivalents deviate from Eq. (16) for $\omega > 10$ due to increasing relative volume of the large spheres with increasing ω[30]. Remarkably, in this range Eq. (16), with swapped values of ϕ_{RCP} and $\nu^{\infty}_{\max}$, fits the data well, as can be seen in Fig. 7(b). The two distinct regimes of $\nu_{\max}$ of bidisperse systems with moderate to large size ratios are predicted by a number of recently published theories[30–33]. A few checks of our bidisperse data with theoretical curves shown in Figure 6 in Ref. 30 show consistency. For a more comprehensive study of the densest binary packing of hard spheres see also Ref. 79.

The reported high-density limit for random close packings[80] is 3% greater than that of Bernal packings[81] and still higher than our ϕ_{RCP} values, and can be approached for extremely fast compression[27,29]. For estimates of ϕ_{RCP} for random close packings of hard spheres see Table 1 in Ref. 82.

Note that the analytical expressions for O_1 and O_2 for two of the considered polydisperse size distributions shown in Appendix E involve power laws and logarithmic functions as in Eqs. (15) and (16), respectively. This suggests that the jamming density in general could be expressed through O_1 and O_2, though we did not investigate this possibility in detail and leave it for further research.

F. Different growth rates

The effect of using different growth rates Γ on the maximum density is shown in the inset of Fig. 7(a) for two size distributions. We observe that the maximum density slightly increases (within 1%) with decreasing the growth rate. There are no signs of saturation for $\Gamma \to 0$, which indicates a quite interesting slow dynamics, leaving plenty of questions open for further research. The effect of using various expansion rates is more comprehensively studied in Refs. 26–29, and 84, so that we do not display more of our data. We did not study extremely slow rates and rate-dependence systematically. We only note that different growth rates can lead to different metastable freezing points[28].

G. Super dense limit

In this subsection we show that sufficiently close to the jamming density, the compressibility factor is independent of the size distribution and depends on only one parameter, the jamming density itself, complementing an earlier study of monodisperse systems[57]. Figure 8 shows the compressibility factor scaled by equation (14) for systems with uniform size distributions.

The jamming densities ϕ_{J} used in Fig. 8 are determined using Eq. (14) by mapping the diverging compressibility factor to finite values, as suggested by Torquato *et al.*[57,85]. It must be noted that all ϕ_{J} differ from $\nu_{\max}$

obtained in simulations by at most 10^{-13}, which confirms that we are close to the infinite pressure limit. We see from Fig. 8 perfect agreement with the free volume theory for all considered systems at the densities $(\phi_J - \nu) \lesssim 10^{-8}$. Only one free parameter is required for the free volume theory, ϕ_J, even though in other studies two fitting parameters are used[24,29]. In order to capture the deviation of the compressibility factor from the free volume theory as the density difference increases, theories which take into account the geometry and structure of the free volume should be developed. The point where data collapse with the free-volume theory is the point where cages are established and do not change any more[86].

It must be noted that the results of Fig. 8 are obtained using numerical double type (8 bytes). We used also long double type (16 bytes) for a few simulations and (while the data in Fig. 8 did not change) could reach perfect agreement with the free-volume theory Eq. (14), using raw data (without ϕ_J mapping), even for $10^{-15} \lesssim (\nu_{max} - \nu) \lesssim 10^{-8}$, i.e., over seven orders of magnitude, which is quite remarkable.

Finally, we remark that even though the free volume theory presented in Eq. (14) is designed for monodisperse systems, we observe a very good agreement for polydisperse systems as well (see Fig. 8). We also confirmed Eq. (14) for two-dimensional systems, and for systems with uniform volume and bidisperse size distributions (data not shown), and for different compression rates.

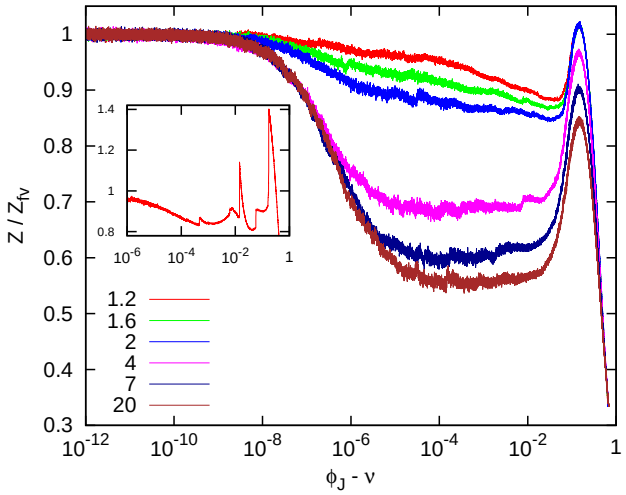

FIG. 8. (Color online) The compressibility factor scaled by the free volume equation of state (14) in the limit of diverging pressure for systems with uniform size distribution for different size ratios, increasing ω corresponds to top-to-bottom, with growth rate $\Gamma = 16 \times 10^{-6}$. When partial crystallization happens we see some fine structures as shown in the inset for the monodisperse system ($\omega = 1$).

IV. SUMMARY AND CONCLUSIONS

In this study we have shown analytically that for any given polydisperse system an equivalent bidisperse system can be constructed with the same equation of state in the fluid regime, using Eqs. (C1) and (C2). In order to confirm this result simulation data of the measured compressibility factor are compared to previously found equations of state and agreement was found with less than 1% deviation. Based on the simulation data a slightly more accurate equation of state (13) was proposed for the fluid regime.

Surprisingly, for densities higher than the freezing (or glass transition) density, beyond the fluid regime, our simulations show that a polydisperse system and its bidisperse equivalent have similar equations of state, i.e., the estimated jamming density is within 1%, as long as the bidisperse systems do not show either (partial) crystallization or (theoretically predicted[30]) change in maximum-density-behavior due to the overwhelming presence of the major species.

We have observed three distinct types of liquid-solid organization / behavior in the bidisperse systems with equal number of small and big particles, depending on the size ratio R^{bi}. First, for $R^{bi} \lesssim 1.1$ the crystalline phase formed at high densities consists of a crystal made of both small and big particles; second, in the range $1.1 \lesssim R^{bi} \leq 2.06$ we do not observe any signs of ordering effects, i.e., an amorphous solid is formed; finally, at moderate to large size ratios $R^{bi} \gtrsim 2.40$, we observe an ordered structure that consists of a crystal of predominately large particles. We confirm this using two different criteria to quantify partial crystallization, i.e., the compressibility factor and the jamming density. Note that above results are obtained using (relatively) slow density growth rates, while for extremely fast compression it is possible to avoid partial crystallization. For the polydisperse systems tested, we find partial crystallization only for (relatively) low size ratios ω, i.e., $\omega \lesssim 1.2$, but not for larger ω.

Sufficiently close to the jamming density the compressibility factor is independent of both size distribution and compression rate and depends only on one free parameter, the jamming density itself. The free volume equation of state (14) is in very good agreement with our simulation results for all considered systems in two- and three-dimensions. We provide analytical (empirical fits) equations for the jamming density as function of the extreme size ratio for uniform size and uniform volume radii distributions to be confronted with theory and experiments.

The result with potential for applications is the fact that polydisperse systems can be modeled[87] by their bidisperse equivalents and their jamming (packing) density can be predicted from the moments O_1 and O_2. Furthermore, the results of this study can be used for better understanding the equation of state for mixtures of fluids and thus, to predict mixing / segregation. Finally, our predictions concerning the size ratios for which crystal-

lization happens can be useful for experiments on colloids and granular media, to either avoid or establish ordering effects.

We would like to stress that this is a preliminary study that considers mostly relatively slow growth rates for a few size distribution function shapes. Whether our predictions also hold for very differently shaped and much wider size distribution functions is open as well as questions about much slower or faster growth rates.

In a future study we will introduce an equivalent tridisperse system and show that with this it is possible to suppress partial crystallization of binary systems also for large size ratios. Comparison with experiment is another subject of future research.

ACKNOWLEDGMENTS

The authors would like to thank Andrés Santos, Martin van der Hoef, Nicolás Rivas, Sebastián González, Fatih Göncü and two anonymous reviewers for helpful suggestions, and Monica Skoge and Aleksandar Donev for consultations about the event-driven code. This research is supported by the Dutch Technology Foundation STW, which is the applied science division of NWO, and the Technology Programme of the Ministry of Economic Affairs, project Nr. STW-MUST 10120.

Appendix A: DERIVATION OF THE EFFECTIVE CORRELATION FUNCTION

In order to express the compressibility factor in the 3D mixtures, using dimensionless moments, plug Eqs. (2), (3) and (4) into the expression in brackets of Eq. (5):

$$\begin{aligned} & g_{11}a_{11}^3n_1^2 + 2g_{12}a_{12}^3n_1n_2 + g_{22}a_{22}^3n_2 \\ & \quad \equiv \frac{1}{1-\nu}(a_{11}^3n_1^2 + 2a_{12}^3n_1n_2 + a_{22}^3n_2) \\ & \quad + \frac{3\nu\frac{A_2}{A_3}}{2(1-\nu)^2}(a_{11}^3n_1^2 + \frac{4}{1+R}a_{12}^3n_1n_2 + \frac{1}{R}a_{22}^3n_2^2) \\ & \quad + \frac{(\nu\frac{A_2}{A_3})^2}{2(1-\nu)^3}(a_{11}^3n_1^2 + \frac{8}{(1+R)^2}a_{12}^3n_1n_2 + \frac{1}{R^2}a_{22}^3n_2^2) \\ & \quad \equiv \frac{6\langle a\rangle\langle a^2\rangle + 2\langle a^3\rangle}{1-\nu} + \frac{6\nu(\langle a\rangle\langle a^2\rangle\langle a^3\rangle + \langle a^2\rangle^3)}{(1-\nu)^2\langle a^3\rangle} \\ & \quad + \frac{4\nu^2\langle a^2\rangle^3}{(1-\nu)^3\langle a^3\rangle}. \end{aligned} \tag{A1}$$

Using the expression (A1), and inserting Eqs. (6), one obtains:

$$\begin{aligned} Z-1 &= (1+r)\frac{\nu}{4\langle a^3\rangle}(g_{11}a_{11}^3n_1^2 + 2g_{12}a_{12}^3n_1n_2 + g_{22}a_{22}^3n_2) \\ &= (1+r)2\nu\frac{(1-\nu)^2 + 3O_1(1-\nu) + O_2(3-\nu)\nu}{4(1-\nu)^3} \\ &= (1+r)2\nu g_{\text{eff}}(\nu), \end{aligned} \tag{A2}$$

where r is the restitution coefficient.

Appendix B: BOUNDS OF DIMENSIONLESS MOMENTS

In order to show that $O_1 \leq 1$, find the extrema of $g(\{a_i\}) = NO_1 = \sum a_i \sum a_i^2 / \sum a_i^3$, $i \in [1, N]$ on the interval $a_i \in (0, \infty)$. For this solve the system of $k = 1, ..., N$ equations:

$$\frac{\partial g(\{a_i\})}{\partial a_k} = \left[\frac{2a_k\sum a_i + \sum a_i^2}{\sum a_i^3} - \frac{3a_k^2\sum a_i \sum a_i^2}{(\sum a_i^3)^2}\right] = 0. \tag{B1}$$

The system (B1) has one (trivial) solution $a_i = a = const$, which corresponds to the monodisperse case. By looking at the sign of the second derivative of $g(a_i = a)$ it can be checked that this extremum is the local maximum $g^{\max} = N$. Therefore the local maximum of O_1 is equal to unity.

By analogy, considering the extrema of the function $f(a_i) = O_2/O_1$, it can be shown that $O_2 \leq O_1$.

Finally, to show that $O_1^2 \leq O_2$, note that $O_1^2/O_2 = A$, where $A = \langle a\rangle^2 / \langle a^2\rangle \leq 1$. This yields $O_1^2 \leq O_2$, where equality is reached only in the monodisperse case ($O_1 = O_2 = 1$).

Appendix C: EQUIVALENT BIDISPERSE SYSTEMS

In order to find a bidisperse system that has the same dimensionless moments O_1 and O_2 as a given polydisperse one, solve analytically the system of equations (6) in terms of the variables n_1 and R. This yields a unique solution ($O_1 \neq O_2$):

$$n_1^{\text{bi}} = \frac{1}{2} + \frac{3O_1O_2 - O_2 - 2O_1^3}{2\lambda}, \tag{C1}$$

$$R^{\text{bi}} = \frac{2O_1^3 + 2O_2^2 + O_2 - 4O_1O_2 - O_1^2O_2 + (1-O_1)\lambda}{2(O_2 - O_1)(O_1^2 - O_2)}, \tag{C2}$$

where $\lambda = \sqrt{O_2}\sqrt{4O_1^3 + O_2 - 3O_1(2+O_1)O_2 + 4O_2^2}$ and n_1^{bi} corresponds here to the number fraction of large particles, i.e., $R^{\text{bi}} \geq 1$. Inserting these values into Eq. (8) leads also to the same compressibility factor $Z^{\text{bi}}(n_1^{\text{bi}}, R^{\text{bi}}) = Z^{\text{poly}}(O_1, O_2)$.

Appendix D: GROWTH RATE

In order to maintain the size distribution during the growing process, the radius a_i of the particle i changes with time as:

$$\frac{da_i}{dt} = \Gamma \frac{a_i}{a_{\max}(t)}, \tag{D1}$$

where $a_{\max}(t)$ is the radius of the largest particle (which depends on time) and Γ is the growth rate with units of velocity. In this convention, we have $a_{\max}(t) = \Gamma t$ and $a_{\min}(t) = \Gamma \omega^{-1} t$, where $a_{\min}(t)$ is the radius of the smallest particle and ω is constant, as desired. This ensures that the relative distribution of radii and thus sphere volumes around the mean is constant over time, but the mean sphere volume increases uniformly with time.

Appendix E: DIMENSIONLESS MOMENTS FOR DIFFERENT SIZE DISTRIBUTIONS

Assume a polydisperse distribution of particle radii with probability $f(a)da$ to find the radius a between radii a and $a + da$, and with $\int_0^\infty f(a)da = 1$. Using the definition of the k-th moment of the size distribution $f(a)$, $\langle a^k \rangle \equiv \int a^k f(a)da$, it is straightforward to calculate dimensionless moments $O_1 = \langle a \rangle \langle a^2 \rangle / \langle a^3 \rangle$ and $O_2 = \langle a^2 \rangle^3 / \langle a^3 \rangle^2$ for any given polydisperse size distribution.

For the uniform size distribution, with $\omega = a_{\max}/a_{\min}$, we obtain:

$$O_1 = 1 - \frac{2}{3}\frac{\omega_0^2}{1+\omega_0^2},\ O_2 = \frac{1}{27}\frac{(3+\omega_0^2)^3}{(1+\omega_0^2)^2}, \tag{E1}$$

where $\omega_0 = (\omega - 1)/(\omega + 1)$, and $2\omega_0 \langle a \rangle$ is the width of size distribution function $f(a)$. It must be noted, that plugging Eq. (E1) into Eq. (C1) yields $n_1^{\text{bi}} = 1/2$. Therefore, a bidisperse system which is equivalent to a polydisperse system with uniform size distribution has the same number of small and large particles for any ω.

For the uniform volume distribution, we have ($\omega > 1$):

$$O_1 = \frac{2\omega}{\omega^2 - 1}\ln\omega,\ O_2 = \frac{2\omega^2}{(\omega-1)^3(\omega+1)}\ln^3\omega. \tag{E2}$$

For examples of numerical values see table I.

The moments of the log-normal distribution (not used in our present simulations) can be computed from the moment generating function of the normal distribution[88]. If X has the log-normal distribution with parameters μ and σ then $\mathbb{E}(X^n) = \exp[n\mu + (1/2)n^2\sigma^2]$, $n \in \mathbb{N}$. Therefore, we obtain:

$$O_1 = \exp(-2\sigma^2),\ O_2 = \exp(-3\sigma^2). \tag{E3}$$

In a number of studies[35,65,66] the magnitude of the spread of sphere radii is conveniently characterized by the parameter δ, which is often also referred to as polydispersity and measures the standard deviation of the radii distribution normalized by its mean: $\delta = (\langle a^2 \rangle - \langle a \rangle^2)^{1/2} / \langle a \rangle$. Therefore we also provide an expression for δ as function of O_1 and O_2: $\delta = (O_2/O_1^2 - 1)^{1/2}$, which is directly related to the parameter A used in Ref. 24, $A = 1/(\delta^2 + 1)$.

Distr.	Figs.	ω	O_1	O_2	R^{bi}	n_1^{bi}	δ
US	1, 2, 3,	1.0	1.0	1.0	1.0		0
	4, 5, 6(a),	1.2	0.995	0.992	1.11		0.05
	7(a), 8	1.4	0.982	0.973	1.21		0.10
		2	0.933	0.903	1.48		0.19
		4	0.824	0.760	2.06		0.35
		5	0.795	0.725	2.25	1/2	0.38
		10	0.733	0.657	2.79		0.47
		20	0.700	0.624	3.19		0.52
		50	0.680	0.605	3.49		0.55
		100	0.673	0.599	3.61		0.57
		∞	2/3	16/27	$2+\sqrt{3}$		$\sqrt{3}/3$
UV	1(d), 6(b),	1.0	1.0	1.0	1.0	1/2	0
	7(b)	1.2	0.994	0.992	1.11	0.453	0.05
		1.4	0.981	0.972	1.21	0.413	0.10
		2	0.924	0.888	1.49	0.327	0.20
		4	0.739	0.632	2.24	0.190	0.39
		5	0.671	0.543	2.56	0.156	0.46
		7	0.568	0.418	3.13	0.114	0.55
		8	0.528	0.373	3.40	0.100	0.58
		10	0.465	0.304	3.90	0.080	0.64
		100	0.092	0.020	17.83	0.006	1.16
		∞	0	0	–	–	–

TABLE I. Given are size ratios ω and dimensionless moments O_1 and O_2 for a few polydisperse systems with uniform size (US) and uniform volume (UV) radii distributions and R^{bi} with n_1^{bi} for their bidisperse equivalents.

[1] S. Chapman and T. G. Cowling, *The mathematical theory of nonuniform gases*, Cambridge University Press, London, 1960.
[2] J. M. Ziman, *Models of Disorder*, Cambridge University Press, Cambridge, 1979.
[3] J. P. Hansen and I. R. McDonald, *Theory of simple liquids*, Academic Press Limited, London, 1986.
[4] ed. T. Pöschel and S. Luding; *Granular Gases*, Berlin, 2001. Springer.
[5] A. Ferguson, B. Fisher, and B. Chakraborty, *EPL*, 2004, **66**(2), 277.
[6] S. Luding, *Nonlinearity*, 2009, **22**(12), R101–R146.
[7] N. Rivas, S. Ponce, B. Gallet, D. Risso, R. Soto, P. Cordero, and N. Mujica, *Phys. Rev. Lett.*, 2011, **106**(8), 088001.
[8] L. D. Landau and E. M. Lifschitz, *Physikalische Kinetik*, Akademie Verlag Berlin, Berlin, 1986.
[9] J. G. Kirkwood, E. K. Maun, and B. J. Alder, *J. Chem. Phys.*, 1950, **18**(8), 1040–1047.
[10] R. J. Buehler, J. R. H. Wentorf, J. O. Hirschfelder, and C. F. Curtiss, *J. Chem. Phys.*, 1951, **19**(1), 61–71.
[11] W. W. Wood, *J. Chem. Phys.*, 1952, **20**, 1334.
[12] Z. Salsburg and W. Wood, *J. Chem. Phys.*, 1962, **37**(4), 798.

[13]B. J. Alder, S. P. Frankel, and V. A. Lewinson, *J. Chem. Phys.*, 1955, **23**(3), 417–419.
[14]B. J. Alder and T. E. Wainwright, *J. Chem. Phys.*, 1959, **31**(2), 459–466.
[15]B. J. Alder and T. E. Wainwright, *Phys. Rev.*, 1962, **127**(2), 359–361.
[16]C. Rascón, L. Mederos, and G. Navascués, *Phys. Rev. Lett.*, 1996, **77**(11), 2249–2252.
[17]B. Doliwa and A. Heuer, *Phys. Rev. Lett.*, 1998, **80**, 4915–4918.
[18]S. Torquato, *Phys. Rev. E*, 1995, **51**(4), 3170–3182.
[19]E. Velasco and L. Mederos, *Phys. Rev. B*, 1997, **56**(5), 2432–2440.
[20]A. Santos, S. B. Yuste, and M. L. D. Haro, *Molec. Phys.*, 1999, **96**(1), 1–5.
[21]P. Richard, L. Oger, J.-P. Troadec, and A. Gervois, *Phys. Rev. E*, 1999, **60**(4), 4551–4558.
[22]H. Löwen In ed. K. R. Mecke and D. Stoyan, *Statistical Physics and Spatial Statistics*, Berlin, 2000. Springer.
[23]S. Luding and O. Strauß in *Granular Gases*, ed. T. Pöschel and S. Luding, Lecture Notes in Physics 564; Springer, Berlin, 2000; pp. 389–409.
[24]S. Luding, *Advances in Complex Systems*, 2002, **4**(4), 379–388.
[25]G. Parisi and F. Zamponi, *Reviews of Modern Physics*, 2010, **82**(1), 789–845.
[26]R. J. Speedy, *Molecular Physics*, 1994, **83**(3), 591–597.
[27]S. Torquato, T. Truskett, and P. Debenedetti, *Phys. Rev. Lett.*, 2000, **84**(10), 2064–2067.
[28]M. Skoge, A. Donev, F. H. Stillinger, and S. Torquato, *Phys. Rev. E*, 2006, **74**(4), 041127.
[29]M. Hermes and M. Dijkstra, *EPL*, 2010, **89**(3), 38005.
[30]R. S. Farr and R. D. Groot, *J. Chem. Phys.*, 2009, **131**(24), 244104.
[31]M. Clusel, E. I. Corwin, A. O. N. Siemens, and J. Brujic, *Nature*, 2009, **460**(7255), 611–615.
[32]I. Biazzo, F. Caltagirone, G. Parisi, and F. Zamponi, *Phys. Rev. Lett.*, 2009, **102**(19), 195701.
[33]M. Danisch, Y. Jin, and H. A. Makse, *Phys. Rev. E*, 2010, **81**(5), 051303.
[34]K. A. Newhall, I. Jorjadze, E. Vanden-Eijnden, and J. Brujic, *Soft Matter*, 2011, **7**(24), 11518–11525.
[35]M. Fasolo and P. Sollich, *Phys. Rev. E*, 2004, **70**(4), 041410.
[36]J. Jenkins and F. Mancini, *Journal of Applied Mechanics - Transactions of the ASME*, 1987, **54**(1), 27–34.
[37]J. Jenkins and D. Yoon, *Phys. Rev. Lett.*, 2002, **88**(19), 194301.
[38]T. Boublík, *J. Chem. Phys.*, 1970, **53**(1), 471.
[39]E. W. Grundke and D. Henderson, *Molecular Physics*, 1972, **24**(2), 269.
[40]L. L. Lee and D. Levesque, *Molecular Physics*, 1973, **26**(6), 1351–1370.
[41]N. Carnahan and K. Starling, *J. Chem. Phys.*, 1969, **51**(2), 635–636.
[42]S. Torquato and S. B. Lee, *Physica A: Statistical Mechanics and its Applications*, 1990, **167**(2), 361–383.
[43]R. D. Kamien and A. J. Liu, *Phys. Rev. Lett.*, 2007, **99**(15), 155501.
[44]G. Mansoori, N. Carnahan, K. Starling, and T. Leland, *J. Chem. Phys.*, 1971, **54**(4), 1523–1525.
[45]T. Boublík and I. Nezbeda, *Collect. Czech. Chem. Commun.*, 1986, **51**(11), 2301–2432.
[46]T. Boublík, *Molecular Physics*, 1986, **59**(2), 371–380.
[47]J. V. Sengers, R. F. Kayser, C. J. Peters, and H. J. White, *Equations of State for Fluids and Fluid Mixtures (Experimental Thermodynamics)*, Elsevier Science, Amsterdam, 1 ed., 2000.
[48]A. H. Alexopoulos and C. Kiparissides, *Chemical Engineering Science*, 2007, **62**(15), 3970–3983.
[49]D. Ballal and A. Lefebvre, *Combustion and Flame*, 1979, **35**(2), 155–168.
[50]P. Bartlett, *Molecular Physics*, 1999, **97**(5), 685–693.
[51]A. Santos, S. B. Yuste, and M. L. de Haro, *J. Chem. Phys.*, 2011, **135**(18), 181102.
[52]M. López de Haro, S. Yuste, and A. Santos in *Theory and Simulation of Hard-Sphere Fluids and Related Systems*, ed. n. Mulero, Vol. 753 of *Lecture Notes in Physics;* Springer Berlin / Heidelberg, 2008; pp. 183–245.
[53]A. Santos arXiv:1202.0672v1 [cond-mat.soft], 2012.
[54]B. D. Lubachevsky and F. H. Stillinger, *J. Stat. Phys.*, 1990, **60**(5/6), 561–583.
[55]A. Kansal, S. Torquato, and F. Stillinger, *J. Chem. Phys.*, 2002, **117**(18), 8212–8218.
[56]A. Donev, S. Torquato, and F. H. Stillinger, *J. Comput. Phys.*, 2005, **202**(2), 737 – 764.
[57]A. Donev, S. Torquato, and F. H. Stillinger, *Phys. Rev. E*, 2005, **71**(1), 011105.
[58]V. Ogarko and S. Luding, *Computer Physics Communications*, 2012, **183**(4), 931 – 936.
[59]Y. Tillé, *Sampling Algorithms*, Springer series in statistics, Springer Verlag, New York, NY, 2006.
[60]M. Kolonko, S. Raschdorf, and D. Waesch, *Granular Matter*, 2010, **12**(6), 629–643.
[61]B. J. Alder and T. E. Wainwright, *J. Chem. Phys.*, 1957, **27**(5), 1208–1209.
[62]E. Zaccarelli, C. Valeriani, E. Sanz, W. C. K. Poon, M. E. Cates, and P. N. Pusey, *Phys. Rev. Lett.*, 2009, **103**(13), 135704.
[63]W. van Megen, S. I. Henderson, S. R. Williams, and I. K. Snook In ed. M. Tokuyama and I. Oppenheim, *Statistical Physics: Experiments, Theories and Computer simulations*, pp. 14–17. World Scientific, Singapore, 1998.
[64]P. N. Pusey, *Journal de Physique*, 1987, **48**(5), 709–712.
[65]P. Bartlett, *J. Phys.: Condensed Matter*, 2000, **12**(8A), A275.
[66]P. Sollich and N. B. Wilding, *Phys. Rev. Lett.*, 2010, **104**(11), 118302.
[67]R. Speedy, *J. Phys.: Condensed Matter*, 1998, **10**(20), 4387–4391.
[68]R. Speedy, *J. Phys.: Condensed Matter*, 1997, **9**(41), 8591–8599.
[69]W. G. Hoover and F. H. Ree, *J. Chem. Phys.*, 1968, **49**(8), 3609–3617.
[70]J. Tobochnik and P. M. Chapin, *J. Chem. Phys.*, 1988, **88**(9), 5824–5830.
[71]D. Frenkel and B. Smit, *Understanding Molecular Simulation*, Academic Press, New York, 2002.
[72]S. R. Williams, C. P. Royall, and G. Bryant, *Phys. Rev. Lett.*, 2008, **100**(22), 225502.
[73]N. Hunt, R. Jardine, and P. Bartlett, *Phys. Rev. E*, 2000, **62**(1), 900–913.
[74]J. V. Sanders, *Philosophical Magazine A*, 1980, **42**(6), 705–720.
[75]S. Hachisu and S. Yoshimura, *Nature*, 1980, **283**(5743), 188–189.
[76]A. B. Schofield, P. N. Pusey, and P. Radcliffe, *Phys. Rev. E*, 2005, **72**(3), 031407.
[77]H. J. Herrmann, R. M. Baram, and M. Wackenhut, *Brazilian Journal of Physics*, 2003, **33**(3), 591–593.
[78]T. Aste and A. Coniglio, *Europhys. Lett.*, 2004, **67**(2), 165–171.
[79]A. B. Hopkins, Y. Jiao, F. H. Stillinger, and S. Torquato, *Phys. Rev. Lett.*, 2011, **107**(12), 125501.
[80]L. V. Woodcock and C. A. Angell, *Phys. Rev. Lett.*, 1981, **47**(16), 1129–1132.
[81]J. Bernal, *Nature*, 1959, **183**(4655), 141–147.
[82]J. G. Berryman, *Phys. Rev. A*, 1983, **27**(2), 1053–1061.
[83]F. Göncü, O. Duran, and S. Luding, *Comptes Rendus Mecanique*, 2010, **338**(10-11), 570–586.
[84]W. S. Xu, Z. Y. Sun, and L. J. An, *European Physical Journal E*, 2010, **31**(4), 377–382.
[85]S. Torquato and F. H. Stillinger, *Rev. Mod. Phys.*, 2010, **82**(3), 2633–2672.
[86]V. Ogarko and S. Luding "Structures in hard-sphere fuids and solids" (unpublished), 2012.
[87]C. Hrenya private communications, 2011.
[88]P. Coles and B. Jones, *Mon. Not. R. astr. Soc.*, 1991, **248**(1), 1–13.